# In situ optical monitoring of Fabry-Perot multilayer structures: analysis of current techniques and optimized procedures

Mael Vignaux, Fabien Lemarchand, Catherine Grezes-Besset, Julien Lumeau

# In-situ optical monitoring of Fabry-Perot multilayer structures: analysis of current techniques and optimized procedures

**M. VIGNAUX,[1,2] F. LEMARCHAND,[1] C. GREZES-BESSET[2] AND J. LUMEAU[1,*]**

*[1] Aix-Marseille Univ, CNRS, Centrale Marseille, Institut Fresnel, Marseille – France*
*[2] CILAS Etablissement de Marseille, 600 avenue de la Roche Fourcade, Pole ALPHA Sud – ZI Saint Mitre, 13400 Aubagne – France*
**julien.lumeau@fresnel.fr*

**Abstract:** Single cavity Fabry-Perot filters are one of the most popular designs for the production of narrow bandpass filters. The usual deposition strategy to create such filters based on optical monitoring at the filter central wavelength is well-known and has proven its strength over decades. We review in this paper the possible optical methods to monitor such a filter during production and analyze their strengths and weaknesses. Then, we discuss a new monitoring procedure, mixing different methods, to minimize the production errors of this filter while maintaining a precise filter centering. This strategy is applied on different bandpass filter designs.

**OCIS codes:** (310.0310) Thin films; (310.4165) Multilayer design; (310.1620) Interference coatings.

## References and links

1. F. Flory, *Thin Films for Optical Systems* (CRC, 1995).
2. H. Angus Macleod, *Thin-Film Optical Filters* (CRC, 2010), Fourth Edition.
3. J. Zhang, A. V. Tikhonravov, M. K. Trubetskov, Y. Liu, X. Cheng, and Z. Wang, "Design and fabrication of ultra-steep notch filters," Opt. Express **21**, 21523-21529 (2013).
4. T. Begou, F. Lemarchand, and J. Lumeau, "Advanced optical interference filters based on metal and dielectric layers," Opt. Express **24**, 20925-20937 (2016).
5. A. Thelen, *Design of Optical Interference Coatings* (Mcgraw-Hill Optical and Electro-Optical Engineering Series, 02/1989).
6. P. Baumeister, "Bandpass filters for wavelength division multiplexing - modification of the spectral bandwidth," Appl. Opt. **37**, 6609-6614 (1998).
7. F. Lemarquis, L. Abel-Tiberini, C. Koc and M. Lequime "400-1000 nm all-dielectric linear variable filters for ultra-compact spectrometers," Proc. International Conference on Space Optics (2010).
8. S. Nazarpour, *Thin Films and Coatings in Biology* (Springer Science & Business Media, 2013).
9. C. Hodgson, and C. Rathmell, "Creating Your Own Bandpass Filter" https://www.semrock.com/Data/Sites/1/semrockpdfs/smk-versachrome-wp.pdf.
10. M. Scherer, J. Pistner, and W. Lehnert, "UV- and VIS filter coatings by plasma assisted reactive magnetron sputtering (PARMS)," in Optical Interference Coatings, OSA Technical Digest (Optical Society of America, 2010), paper MA7.
11. M. Lequime, R. Parmentier, F. Lemarchand, and C. Amra, "Toward tunable thin-film filters for wavelength division multiplexing applications," Appl. Opt. **41**, 3277-3284 (2002).
12. H. A. Macleod, "Turning value monitoring of narrow-band all-dielectric thin-film optical filters," Opt. Acta **19**, 1–28 (1972).
13. R Herrmann, A Zoller, "Automated optical coating processes with optical thickness monitoring," Proc. SPIE **0652** (1986).
14. R. R. Willey, "Simulation comparisons of monitoring strategies in narrow bandpass filters and antireflection coatings," Appl. Opt. **53**, A27-A34 (2014).
15. B. T. Sullivan and J. A. Dobrowolski, "Deposition error compensation for optical multilayer coatings. I. Theoretical description," Appl. Opt. **31**, 3821-3835 (1992).
16. M. Lequime, S. Nadji, D. Stojcevski, C. Koc, C. Grezes-Besset, and J. H. Lumeau, "Determination of the optical constants of a dielectric layer by processing in situ spectral transmittance measurements along the time dimension," Appl. Opt. **56**, C181-C187 (2017).
17. H. Krol, C. Grèzes-Besset, D. Torricini, D. Stojcevski, "High performances optical coatings with dual ion beam sputtering technique," Proc. SPIE **9627**, 96270L (2015).
18. A. V. Tikhonravov and M. K. Trubetskov, "Automated design and sensitivity analysis of wavelength-division multiplexing filters," Appl. Opt. **41**, 3176-3182 (2002).

19. M. Trubetskov, T. Amotchkina, and A. Tikhonravov, "Automated construction of monochromatic monitoring strategies," Appl. Opt. **54**, 1900-1909 (2015).
20. R. R. Willey, "Monitoring error compensation in general optical coatings," Appl. Opt. **48**, 4475-4482 (2009).

## 1. Introduction

### *1.1 Thin film Fabry-Perot filters*

Thin film filters offer a wide range of possible optical functions with the advantage that they can be easily integrated into any optical system [1]. From dielectric mirrors [2] to notch filters [3], they have become really powerful and commonly used components when control of spectral properties of light is required. Over the past 15 years, with recent improvements of thin film technology, spectral properties requirements of the final components have become more stringent, thus severely increasing the complexity of the filters to be fabricated.

Designing and fabricating thin film filters is then a recurring compromise between the choice of materials (mainly defined by the spectral region of the application), the technology used for the production (mainly defined by the geometry/nature of the substrate and the materials to deposit) and the required specifications (type of optical function, uniformity, stress…). These choices directly affect the final complexity of the filter to be fabricated and therefore the success yields. As an example, fabricating non absorbing filters for near-UV region requires using materials with larger band-gap for the high index materials (i.e. replacing $Nb_2O_5$ with $HfO_2$), thus resulting in a lower refractive index contrast between high and low index materials and a larger number of layers to be deposited. Despite this designs complexity, and except for very uncommon spectral filters [4], typical structures exist to fulfill certain functions such as bandpass filters, high-pass and low-pass or antireflection coatings [5].

Bandpass filtering, widely used for WDM [6], space applications [7], biophotonics [8], is one of the most popular optical functions that is produced using optical interference coatings. It allows light to be highly transmitted inside a given spectral region (from a few tens of picometers up to hundreds of nanometers) and to reject a specific spectral interval surrounding it. Specifications should include at least the transmitted and the rejected spectral ranges, but also the required level of transmittance inside these ranges and the steepness of the filter at transitions between high and low transmission.

Different ways exist to reach such a spectral response. One method consists in combining shortwave-pass and a longwave-pass filters [9], but the most common one is based on the use of Fabry-Perot structures which offers in one single structure both the narrow bandpass and the rejection bands. A Fabry-Perot filter can be considered as a resonant cavity with a resonating layer, called spacer layer of optical thickness multiple to the half of the resonance wavelength surrounded with two identical reflectors (generally composed with dielectric mirrors also centered at the resonance wavelength). A typical all-dielectric Fabry-Perot structure is:

$$Glass\,|\,\left(HL\right)^q 2pH\ \left(LH\right)^q\,|\,Air\ or\ Glass\,|\,\left(HL\right)^q H\ 2pL\ \left(HL\right)^q H\,|\,Air. \qquad (1)$$

where H and L stand for layers with a quarter wave optical thickness and respectively a high and a low refractive index. q and p are integers. q is related to the mirror reflection efficiency and p is the order of the half wave spacer layer, possibly a high (H) or low (L) index layer. Spectral bandwidth of the filter ($FWHM_\lambda$), in case of a high (H) index spacer layer, is [2]

$$FWHM_\lambda = 2\lambda_0 \frac{n_s}{p\pi n_H}\left(\frac{n_L}{n_H}\right)^{2q+1}. \qquad (2)$$

where $n_H$ and $n_L$ stand for the high and low refractive index, $n_s$ is the glass substrate refractive index and $\lambda_0$ the central wavelength of the filter. Once materials are chosen, the easiest way to

obtain a required $FWHM_\lambda$ is to modify the mirror reflection efficiency by changing the value of q. In addition, most of the time, a squared shaped bandpass is required. It enables to secure high transmission not only at a single wavelength $\lambda_0$, but over a transmission spectral range surrounding $\lambda_0$. This can be done by depositing not just a single Fabry-Perot cavity, but multiple cavities separated with a coupling low index quarter wave layer. By increasing the number of cavities, spectral steepness is increased, leading to a more squared profile. However, Eq. (2) giving the $FWHM_\lambda$ remains valid.

Another important aspect is the rejection band. Fabry-Perot structures present a minimum of level of transmittance directly linked to the mirror reflection efficiency. The width of this rejection band is roughly equal to the width of the reflection band of the mirrors (typically a few hundreds of nanometers) and depends on the ratio of the high and low refractive index materials. If a wider spectral band is required, for example covering the whole sensitivity range of a Si sensor for visible filters [10], Fabry-Perot structures are combined with additional mirrors or edge filters that allow increasing the rejection band to several hundreds of nanometers. These blocking multilayer structures are generally coherently combined with the Fabry-Perot filters within one single structure; however, the final performances over a wide spectral range are highly dependent on the initial performances and especially on errors on each layer of the Fabry-Perot filter that is manufactured.

### *1.2 Optical monitoring and difficulties of manufacturing Fabry-Perot structures*

If design of a conventional Fabry-Perot filter is a fairly easy step, manufacturing and above all, agreement between specifications and measured performances can yield amazing results. In the case of a single cavity Fabry-Perot filter, the most obvious effect is the inaccuracy of the centering wavelength and that thickness errors on each layer introduce a spectral shift depending on the position of the layer. Spacer layer is well known as the most sensitive; so, when considering errors only on this specific spacer layer, the relative spectral shift $\Delta\lambda/\lambda$ is proportional to the relative error on the spacer thickness with a coefficient $\kappa$ always lower than 1 that depends on the dispersion of the phase at reflection of the mirrors. Depending on p and q (values of Eq. (1)) and on the refractive indices, Lequime and al. have shown that for standard configurations, $\kappa$ is in the [0.2-1] range [11]. Under these conditions, a 1% thickness change of the spacer layer will induce a spectral shift ranging from 0.2 to 1%, which corresponds to a deviation value of 0.8 to 10 nm in the [400-1000] nm range. This deviation cannot be neglected compared to the $FWHM_\lambda$ of the filter for narrow band applications. For multiple cavity filters, a spectral mismatch between cavities, leading to a difference of centering between cavities, drastically modifies the resulting spectral transmittance and the squared shape is not reached anymore. All these elements explain why a method with self-compensation is mandatory for Fabry-Perot thin film filters monitoring.

Turning Point Monitoring (TPM) [12] is widely recognized as a powerful self-compensation monitoring method. It consists in measuring the evolution of transmission with deposition time, generally at each rotation of the substrates holder and at a specific wavelength. The deposition is stopped when the signal reaches a maximum or a minimum value of transmission. For monitoring all quarter wave designs such as Fabry-Perot filters, TPM is thus a direct measurement of the transmitted signal at the central wavelength of the multilayer. To increase sensitivity of the method, the signal to noise ratio is generally improved by pre-filtering measured signal, and the derivative versus time is calculated. A signal extremum coincides with a sign change of the derivative, and it is then necessary to calculate, at each instant, the remaining time before the signal derivative is zero. The determination of the stopping moment may be biased by several parameters, including fluctuations of the deposition rate, signal to noise ratio or the dynamics of the signal at the end of the layer.

TPM has proven to be an efficient error self-compensation method. Stopping at a turning point wavelength at each layer enables the argument of the Fresnel reflected coefficient (that

we call hereafter phase φ) to be close to 0 [π]. As described in [2], since φ is self-compensated each time a layer is deposited, the spectral filter centering is maintained layer after layer. TPM does not avoid errors on the thickness of each individual layers, but permits one error to be partially compensated with the deposition of the following layer. More precisely, TPM is not known as a method leading to a low thickness-error mean value, but as an excellent spectral centering method.

However, it is important to mention is that TPM is difficult to apply as soon as the initial part of the stack becomes highly reflective. This is for example the case of monitoring a spacer layer of very narrow bandpass filter which has a very low transmission and a low signal dynamic. In such case, another monitoring method is needed if an all optical monitoring is desired. To achieve this, level-cut monitoring [13] can be considered. Similarly to TPM, it consists in measuring the transmitted signal at a specific wavelength, but, in this case, the deposition is stopped when a pre-calculated transmittance level is reached. This theoretically calculated value does not take into account thickness errors on previous layers, resulting in a non-negligible risk that the target signal is never achieved. In practice, this means that it is generally preferable to choose monitoring wavelengths where the end of the layer does not correspond to the vicinity of an extremum of transmittance. For each layer inside the stack, it is thus optimal to choose a wavelength where the level of transmittance significantly varies at the end of the layer, with a high enough signal dynamic, to minimize the impact of measurement noise. However, as level-cut is sensitive to previous thickness errors, and also to refractive index variations or errors, it has been widely replaced by an improved version called Percent Optical Extremum Monitoring (POEM). R. Willey [14] described this strategy far less sensitive to errors of index or photometric scale. The POEM strategy consists in stopping the layer at a specified percentage of the transmittance evolution determined between the two previous extrema. The extrema do not need to be in the same layer, but should be measured at the same wavelength. Similarly to level-cut, the choice of the monitoring wavelength should correspond to a high dynamic of the signal at the end of the layer in order to reduce thickness errors. As this method relies on percentage of signal dynamics, it is less sensitive than level-cut to previous deposition errors or index mismatch, and thus can be categorized as a partial error compensating method. It has been proven that the thickness-error mean value of a filter monitored by POEM strategy is quite low, and that this method is a good candidate for monitoring complex filters.

## 2. Comparison of monitoring strategies on cavity Fabry-Perot filters

### *2.1 VDP software and parameters*

In order to compare different monitoring strategies, we developed a Virtual Deposition Process algorithm [15]. This software simulates the main error sources of a monitoring system and processes the signals in an identical way. The deposition rate of the two materials is set to 0.1 nm/s. Assuming a substrates holder rotation of 60 rotations per minute, the Virtual Deposition Process generates a discontinuous signal incremented every second, which corresponds to a 0.1 nm increase of the layer thickness. This configuration is then a realistic simulation of a classic optical system performed on a peripheral monitoring test glass.

For the first layer, at each acquisition time, the theoretical signal is calculated using thin films theory and then slightly modified adding a Gaussian noise with standard deviation $\sigma_{Transmittance}$ = 0.006 corresponding to the noise level measured at 600 nm on the monochromatic optical system developed in our facility [16]. Then, when a predetermined trigger value (POEM) or a turning point (TPM) is obtained, the virtual deposition process determines the corresponding thickness. At layer achievement, the thickness of first layer which may differ from the theoretical value is recorded in Virtual Deposition Process and used for the following calculation. The transmitted signal simulating the deposition of the second layer is calculated using this thickness value, and then the Gaussian noise is added to

the theoretical signal as previously explained. In these new conditions and based on the expected signal of the initial structure, the software dynamically determines the stopping time of layer number 2. This process is repeated until complete simulation of stack deposition is achieved. It takes into account cumulative errors, similarly to real deposition conditions. Apart from these optical signal fluctuations, no other source of errors was taken into account in our simulations. In particular, no refractive index errors were considered, and the deposition rate of the materials was supposed to be constant. These suppositions made our simulations reliable on very stable deposition processes such as Dual Ion Beam Sputtering [17] or Plasma-Assisted Reactive Magnetron Sputtering [4,10]. Finally, as a statistical approach including many trials is required for a rigorous comparison of the efficiency of different monitoring strategies, one hundred simulations were typically run for each strategy presented in this paper.

TPM was calculated using the method presented in [18]. At each acquisition, the stopping time is evaluated using an a priori information, the second derivative of transmittance at the turning point and a fitting parameter that minimizes a linear fit of the derivative of transmittance versus time on the 10 last evaluated points. The simulation of monitoring is only active inside a range of thickness of ± 10 nm centered on the nominal thickness. Imposing such boundaries is quite usual on TPM systems to prevent false stops. TPM should be avoided for layers where signal dynamics is weak as it could lead to inaccurate and inconsistent stopping time. The Virtual Deposition Process software allows simulating a quartz microbalance system monitoring for these specific layers with a Gaussian distribution of thickness. The quartz standard deviation is chosen to $\sigma_{thickness}$ = 2 nm.

Finally, for the calculation of the best POEM wavelength, or the best set of wavelengths if required, we developed a specific module on the Virtual Deposition Process software that allows determining them by minimizing several constraints including cumulative effect of thickness errors, a minimal amplitude of the signal variation inside a layer and a minimum distance between the trigger point and the next turning point [19]. The choice between all the wavelengths following these constraints is made by the optimization of a merit function defined by the sum of all the signal derivative (or dynamics) at the end of each layer [19].

### *2.2 First example : single cavity filter*

In our study, we first analyzed an all-dielectric-single-cavity 21-layer Fabry-Perot filter made of two mirrors composed with 10 alternated low and high refractive index materials quarter-wave layers, and a cavity made with a half-wave high index spacer with formula:

$$Glass\left|\ (HL)^5\ 2H\ (LH)^5\right|Air. \tag{3}$$

corresponding to the case p = 1 and q = 5 in Eq. (2). In our numerical study, we considered non dispersive and absorption free materials. However, results can be easily generalized to low absorbing and dispersive materials as soon as the laws governing absorption and dispersion are well-known. The glass index was: $n_S = 1.52$ and the high and low index materials: $n_H = 2.35$ and $n_L = 1.45$. The centering wavelength was $\lambda_0 = 600$ nm.

The theoretical spectral response of this filter was set as our reference. We then simulated the manufacturing of Fabry-Perot filters using different monitoring strategies and compared their final spectral transmissions with the reference. Rather than evaluating a merit function on a whole spectral interval that may be very sensitive to a small spectral shift of the transmittance and does not easily represent the overall performances of a filter over a broad spectral range, we considered several characteristic data of the filter. These characteristic data, schematically represented in Fig. 1, include central wavelength and the corresponding transmittance, spectral bandwidth (Full Width at Half Maximum), minimum values of transmittance inside the rejection band and the corresponding wavelengths, and finally the

two wavelengths corresponding to the boundaries of the rejection band where transmittance is equal to 0.1.

The transmittance at the central wavelength $\lambda_0$ is T = 0.957 and corresponds to a bare substrate (without backside reflectance). This is due to the fact that the structure is based on quarter wave layers with no antireflective coating added on the coating. This value is generally quite stable when introducing thickness errors on each layer as, for a single cavity Fabry-Perot filter, the maximum of transmittance is only sensitive to a difference of the reflectance efficiency between the two mirrors surrounding the spacer layer, at the resonance wavelength. In our case, given considered materials and structure, these mirrors are relatively broadband and stable.

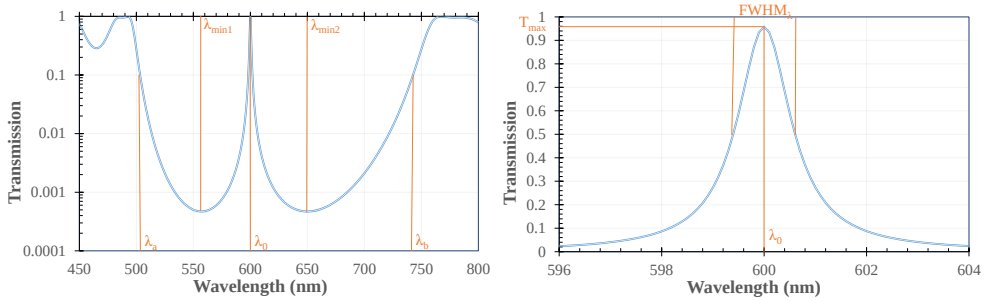


Fig. 1. Typical parameters characterizing the spectral response of a single cavity Fabry-Perot filter. $\lambda_0$ is the central wavelength, $FWHM_\lambda$ is the spectral bandwidth, $\lambda_{min1}$ and $\lambda_{min2}$ the two wavelengths where the transmittance are minimal, $\lambda_a$ and $\lambda_b$ the two wavelengths corresponding to the end of the rejection band (transmittance = 0.1).

The results for the nominal 21-layer filter are given in Table 1.

**Table 1. Nominal values of the 9 parameters described in Fig. 1**

| $\lambda_0$ nm | $T(\lambda_0)$ 0-1 | $FWHM_\lambda$ nm | $T_{max}$ 0-1 | $\lambda_{min1}$ nm | $T(\lambda_{min1})$ 0-1 | $\lambda_{min2}$ nm | $T(\lambda_{min2})$ 0-1 | $\lambda_a$ nm | $\lambda_b$ nm |
|---|---|---|---|---|---|---|---|---|---|
| 600 | 0.957 | 1.21 | 0.957 | 557.20 | $4.7\ 10^{-4}$ | 650.10 | $4.7\ 10^{-4}$ | 503.3 | 742.7 |

The $FWHM_\lambda$ is calculated, not for its intrinsic value, but as a reference to qualify a possible spectral shift of the central wavelength position $\lambda_0$ (maximum allowable shift not exceeding a fraction of $FWHM_\lambda$). $\lambda_{min1}$, $\lambda_{min2}$, $\lambda_a$ and $\lambda_b$ are characteristics of the spectral behavior outside the bandpass. These data will allow characterizing the effect of a single wavelength error compensation monitoring method on broadband properties of Fabry-Perot filters. An accurate comparison of different monitoring strategies should rely on a statistical approach with enough different trials to give conclusions. For every tested strategy, we thus considered 100 different predictions, assessed the average value and the standard deviation for each parameter listed in Table 1/Fig. 1 and finally analyzed these data. If the average value is very close to the nominal one, it is characteristics of a strategy inducing no bias on the value of the considered parameter. The standard deviation is the result of the noise related signal fluctuations on the monitoring strategy, and a low value is characteristics of a robust and reproducible strategy.

In order to qualify a strategy, we propose to consider a strategy valid for a given parameter if more than 95% of the trials give a value inside an acceptable interval (i.e. values of each parameter at twice the standard deviation). Within our study, we considered that:

- a spectral shift of $\lambda_0$ below 0.12 nm, i.e. one tenth of $FWHM_\lambda$ is – from the end-user point of view – acceptable for a given monitoring method,
- $\lambda_{min1}$, $\lambda_{min2}$ must differ from their nominal value by less than 1 nm,
- $\lambda_a$ and $\lambda_b$ , must differ from their nominal value by less than 2 nm.

These values will secure that the spectral response both close and far from the Fabry-Perot resonance is matching the theoretical one.

As a starting point, we first consider TPM strategy at the central wavelength of the Fabry-Perot filter, i.e. 600 nm. To avoid errors associated with low signal dynamic, we suppose that layers 10, 11 and 12, corresponding to the spacer and surrounding mirrors layers are monitored in physical thickness with a quartz crystal microbalance. Table 2 lists the calculated mean value differences and standard deviations of the considered parameters for a TPM strategy using the resulting spectral simulations over 100 virtual depositions. Note that all calculations were carried out with a fixed window and that TPM strategy could be improved by optimizing the calculation window for each layer. With TPM, the centering wavelength is very stable as predicted by the turning point error compensation effect.

**Table 2. Mean value (upper data), mean value difference (data into brackets) and standard deviation of the 9 parameters listed in Table 1 using a TPM strategy. A wavelength parameter is validated if more than 95% of the predictions are inside a predefined interval.**

| | $\lambda_0$ nm | $T(\lambda_0)$ 0-1 | $FWHM_\lambda$ nm | $\lambda_{min1}$ nm | $T(\lambda_{min1})$ 0-1 | $\lambda_{min2}$ nm | $T(\lambda_{min2})$ 0-1 | $\lambda_a$ nm | $\lambda_b$ nm |
|---|---|---|---|---|---|---|---|---|---|
| Mean Value | 600.003 | 0.961 | 1.222 | 556.84 | $4.610^{-4}$ | 649.47 | $4.9310^{-4}$ | 502.7 | 742.2 |
| Difference | (0.003) | (0.004) | (0.012) | (-0.358) | ($-7.8\ 10^{-6}$) | (-0.627) | ($2.3\ 10^{-5}$) | (-0.59) | (-0.504) |
| 2 × Standard deviation | <0.001 | 0.008 | 0.024 | 1.814 | $7.6\ 10^{-5}$ | 1.830 | $6.8\ 10^{-5}$ | 3.728 | 5.446 |
| Validation | **Yes** | - | - | No | - | No | - | No | No |

The mean value difference is acceptable for the 5 wavelength parameters, showing low systematic error on our simulations. However, $\lambda_{min1}$, $\lambda_{min2}$ and mostly $\lambda_a$ and $\lambda_b$ present a high statistical standard deviation, typical of widely dispersive values. TPM is a monochromatic error compensation method. Therefore as soon as the wavelength differs from the monitoring wavelength, (i.e. 600 nm), individual layers thickness errors can induce drastic spectral effects, making this strategy fully useful when only interested in the bandpass domain. In conclusion, TPM strategy allows achieving high accuracy close to the bandpass region but results in large discrepancies far from these regions (as shown by the unacceptable large dispersion values of the four spectral parameters $\lambda_{min1}$, $\lambda_{min2}$, $\lambda_a$ and $\lambda_b$).

We then analyzed the result of a single cavity Fabry-Perot filter when using POEM strategy. In order to achieve best result for production, the proper choice of the monitoring wavelength is critical. Optimal wavelength for a monochromatic POEM strategy, respecting various constraints and maximizing a merit function as described in section 2.1, was calculated by the Virtual Deposition Process dedicated module to be 493 nm. However, it can be shown that when using single monitoring wavelength, the stopping criteria of the last two layers are critically approaching a TPM, making single wavelength POEM strategy a non-optimal technique. It is thus interesting to authorize a second POEM monitoring wavelength resulting in a significant improvement of the merit function by 60%. The strategy then consists in monitoring layers 1 to 19 at 493 nm and the two final layers 20 and 21 at 450 nm. It is worth noting that no noticeable improvement was obtained by authorizing a third POEM wavelength.

Statistical results using POEM are listed in Table 3. The influence of the signal noise causes an average value difference of the filter centering about 0.2 nm and a standard deviation slightly above 0.4 nm, i.e. too high for validating the strategy. However, all the other four calculated wavelength parameters are acceptable, considering either their mean value or standard deviation. We can interpret these results as the ability of POEM to give a good global spectral agreement. However, this method is not compatible with narrow bandpass filtering applications where a perfect centering of the bandpass is required. To better understand these results, it can be noticed that whatever the monitoring method, a good

accordance of the spectral response over a wide spectral range requires very low thickness error on each individual layer: in other words, compensating a relatively large thickness error of a previous layer by adjusting the thickness of the subsequent layers does not allow producing a filter with spectral response matching the theoretical one on a broad spectral domain. POEM clearly appears as a much better technique than TPM for minimizing thickness error of each individual layer. On the other hand, an accurate wavelength centering of the transmitted bandpass only depends on the value of the final phase of the Fresnel complex amplitude coefficient φ. The central wavelength thus corresponds to the wavelength where φ is equal to 0. POEM principle does not take into account the phase value at 600 nm. Centering of the filter is thus restricted to the phase error at 600 nm resulting from the thickness error of each individual layer. In contrary, TPM relies on stopping deposition as soon as a phase φ equal to zero is achieved for the partial stack, layer after layer. Therefore TPM is a method that ensures not only the final value of φ to be close to zero but also a null value of intermediate phases calculated at the end of each layer.

**Table 3. Mean value (upper data), mean value difference (data into brackets) and standard deviation of the 9 parameters listed in Table 1 using a POEM strategy. A wavelength parameter is validated if more than 95% of the predictions are inside a predefined interval.**

| | $\lambda_0$ nm | $T(\lambda_0)$ 0-1 | $FWHM_\lambda$ nm | $\lambda_{min1}$ nm | $T(\lambda_{min1})$ 0-1 | $\lambda_{min2}$ nm | $T(\lambda_{min2})$ 0-1 | $\lambda_a$ nm | $\lambda_b$ nm |
|---|---|---|---|---|---|---|---|---|---|
| Mean Value | 600.2 | 0.955 | 1.213 | 557.18 | $4.62\ 10^{-6}$ | 649.95 | $4.63\ 10^{-6}$ | 503.18 | 742.51 |
| Difference | (0.200) | (-0.002) | (0.003) | (0.014) | ($-7.7\ 10^{-6}$) | (-0.150) | ($7.1\ 10^{-6}$) | (-0.122) | (-0.188) |
| 2 × Standard deviation | 0.848 | 0.004 | 0.004 | 0.342 | $1.76\ 10^{-5}$ | 0.476 | $1.56\ 10^{-5}$ | 0.074 | 0.114 |
| Validation | No | - | - | **Yes** | - | **Yes** | - | **Yes** | **Yes** |

In order to find a strategy permitting both an accurate centering of the bandpass and a low deviation of the broadband spectral response, we opted to take the best of each previously described methods and to combine them: the beginning of the monitoring is carried out with POEM strategy to minimize the error of each individual layer and TPM is then used to terminate the deposition in order to secure a proper final phase at achievement. However the determination of the optimal layer for changing the monitoring strategy is critical for obtaining optimal results. First of all, it would be fallacious to introduce TPM only for the last layer. Indeed, the sensitivity of the Fabry-Perot filter phase is maximal for the spacer layer and decreases as soon as the considered layer is far from the spacer one. The filter centering with the only last layer is certainly possible, but the necessary thickness correction would be so high that the transmission behavior over a broad spectral range would be strongly affected. Moreover, it is not a good strategy to introduce TPM near the most sensitive layers. While phase correction could be obtained with minimal adjustment of the layer thickness, the signal modulation near the spacer layer is too weak for a precise monitoring taking into account some noise. It is thus mandatory to develop a specific technique for determining the optimal layer for switching the strategy. Our approach consisted in simulating, using Virtual Deposition Process, layer after layer, the phase error of a partial filter, for POEM and TPM methods. This phase error study is a good indicator of the strategy capacity to maintain the filter centering during its construction while keeping minimal errors on each individual layer thickness. In order to make a statistical study of the phase, we considered the phase Root Mean Square Deviation given by:

$$\varphi_{RMSD} = \sqrt{\frac{\sum_{i=1}^{Npr} \left(\varphi(i) - \varphi_{th}\right)^2}{Npr}}. \qquad (4)$$

where $\varphi_{th}$ is the theoretical reflection phase of the filter at the end of a layer , $\varphi(i)$ the phase of the i$^{th}$ simulated filter, and $Npr$ =100, the number of predictions. Note that for quarterwave designs, $\varphi_{th}$ is equal to zero or $\pi$. Figure 2 describes the statistical approach (100 predictions) of $\varphi_{RMSD}$ at 600 nm at the end of each layer during the construction of the filter using TPM method. $\varphi_{RMSD}$ integrates information both on the statistical and systematic deviation of phase values. The $\varphi_{RMSD}$ value is directly influenced by the degree of noise added to the signal, but also depends on the turning point's calculation method, and on the signal dynamics at the end of the layer. $\varphi_{RMSD}$ is below 2 degrees for layers 1-9 and the low index layers 14, 16, 18, and 20. $\varphi_{RMSD}$ increases up to 15 degrees for the spacer which is quartz monitored (layers 10 and 12 are also supposed to be quartz monitored). It is worth noting that TPM being a phase compensation method, it should be able to maintain a proper centering of the whole filter at the end of each layer. Consequently, the high values of $\varphi_{RMSD}$ obtained at the end of some specific layers (Fig. 2) are directly linked to difficulties to monitor these specific layers. This is the case for layers 13, 15, 17 or 19 for which the transmission is quickly evolving at the very end of the last layer (large $\left|\partial^2 T / \partial^2 t\right|$ ) resulting in a difficulty to anticipate the position of the turning point.

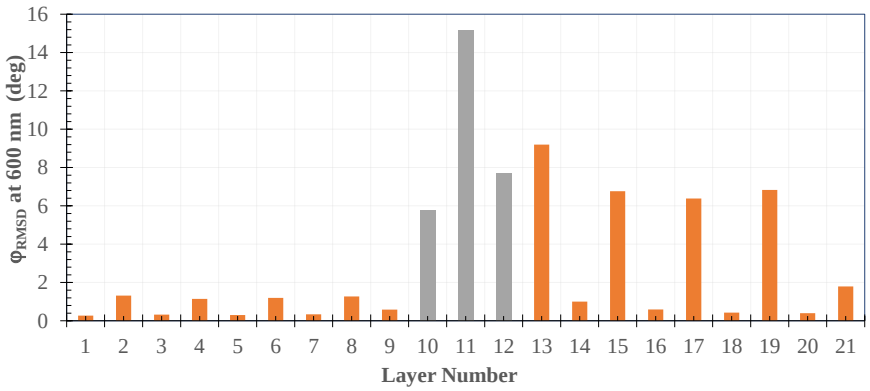


Fig. 2. $\varphi_{RMSD}$ calculated at the end of each layer using TPM strategy and 100 predictions. Grey rectangles correspond to Quartz monitoring and orange ones to TPM.

In the case of the POEM strategy, we have already shown that no phase compensation occurs at 600 nm, whatever the trigger wavelength. Hence, $\varphi_{RMSD}$ is a good indicator of the average global thickness error of all previous layers controlled by POEM. It is expected that, as the average thickness error increases layer after layer, the value of $\varphi_{RMSD}$ also increases with the number of layers. In Fig. 3, we plotted the evolution of $\varphi_{RMSD}$, at 600 nm, calculated at the end of each layer, for different monochromatic POEM wavelengths ranging from 480 to 510 nm.

The wavelength range in Fig. 3 was restricted to the useful range, as the calculation on a wider one did not provide better results. The displayed layers were also restricted from layer 1 to layer 14 as for layer 15 to 21, the value of $\varphi_{RMSD}$ exceeds acceptable values whatever the considered wavelength. Data of Fig. 3 illustrate the capability of POEM strategy to maintain a low $\varphi_{RMSD}$ value, and consequently, the filter centering at 600 nm, with performances comparable to a TPM, if proper monitoring wavelength is chosen. For the first layers, POEM appears as an optimal monitoring procedure as it induces even less phase error than TPM. POEM applied at the specific wavelength 497 nm permits to maintain $\varphi_{RMSD}$ below 3.5 degree from layer 1 to 14, significantly lower than the average value obtained with TPM. This is due to very low thickness errors induced by POEM at the beginning of the filter. Then, when the number of layers increases, the limited phase compensation phenomenon associated

with POEM becomes problematic. At layer 15, $\varphi_{RMSD}$ value obtained by POEM is 8.5 degree and becomes larger than the 6.8 degree obtained when using TPM. Consequently, the centering of a partial filter (from layer 1 to 14) monitored by a 497 nm POEM is more or less equivalent in terms of centering as the same filter monitored by 600 nm TPM. However, as such a filter presents a lower average thickness error for each individual layer, the agreement of the spectral behavior over a broad spectral domain is better than with TPM only. As soon as POEM becomes less efficient than TPM to monitor $\varphi_{RMSD}$, it becomes then optimal to switch to TPM technique for the monitoring of layer 15 to 21 (hybrid optical monitoring technique). Finally, by terminating the filter manufacturing using TPM, optimal centering of the complete final filter is ensured.

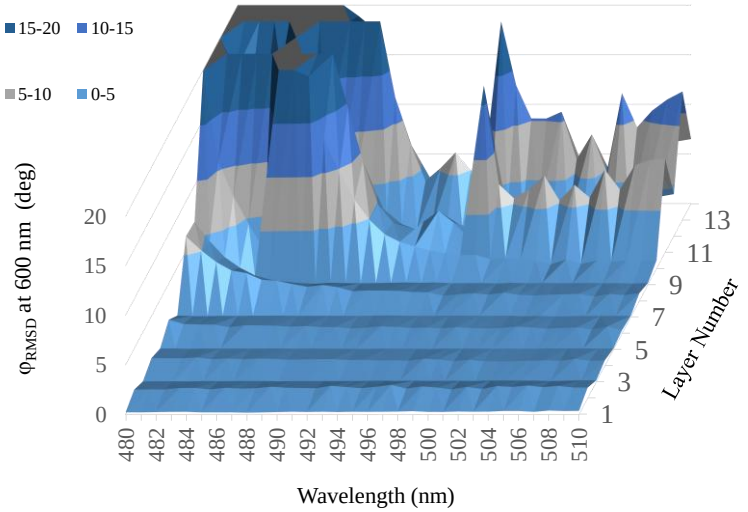


Fig. 3. $\varphi_{RMSD}$ calculated at the end of layer 1 to 14 using POEM strategy in the 480-510nm range and based on 100 predictions.

Table 4 lists the mean value difference and the standard deviation of the 9 parameters defined in Fig. 1 for the hybrid 497 nm POEM (layers 1 to 14) / 600 nm TPM (layers 15 to 21) monitoring strategy. It can also be noted that all data are compliant with requirements, and that, in this case, the hybrid strategy enables to combine the benefits of each technique, i.e. to obtain an excellent filter centering similar to complete TPM strategy and a fair broadband spectral agreement similar with complete optimal POEM strategy.

**Table 4. Mean value (upper data), mean value difference (data into brackets) and standard deviation of the 9 parameters listed in Table1 using a hybrid strategy. All the wavelength parameters are validated with more than 95% of the predictions inside the predefined interval.**

| | $\lambda_0$ nm | $T(\lambda_0)$ 0-1 | $FWHM_\lambda$ nm | $\lambda_{min1}$ nm | $T(\lambda_{min1})$ 0-1 | $\lambda_{min2}$ nm | $T(\lambda_{min2})$ 0-1 | $\lambda_a$ nm | $\lambda_b$ nm |
|---|---|---|---|---|---|---|---|---|---|
| Mean Value | 600.002 | 0.957 | 1.212 | 556.97 | $4.53\ 10^{-4}$ | 649.85 | $4.52\ 10^{-4}$ | 502.57 | 742.34 |
| Difference | (0.002) | (<0.001) | (0.002) | (-0.231) | ($-1.7\ 10^{-5}$) | (-0.246) | ($1.8\ 10^{-5}$) | (-0.728) | (-0.361) |
| 2 x Standard deviation | <0.001 | <0.001 | <0.001 | 0.196 | $7.2\ 10^{-6}$ | 0.192 | $6.6\ 10^{-6}$ | 0.382 | 0.566 |
| Validation | **Yes** | - | - | **Yes** | - | **Yes** | - | **Yes** | **Yes** |

One important remark concerns the difference of calculation methods used to determine the POEM wavelength. Whereas for POEM strategy, the 493 nm wavelength was calculated using a Virtual Deposition Process additional module based on some considerations on the transmitted signal behavior (dynamics, distance to turning point), our hybrid strategy, based

on the phase error minimization, integrates both supposed signal noise and main target of the filter, i.e. the necessity to maintain a good filter centering layer after layer. In other terms, a POEM strategy integrates general considerations inherent to all kind of filters while the hybrid strategy, as described below, is dedicated to bandpass filtering and takes into account specific monitoring technique inherent errors associated with a given signal noise.

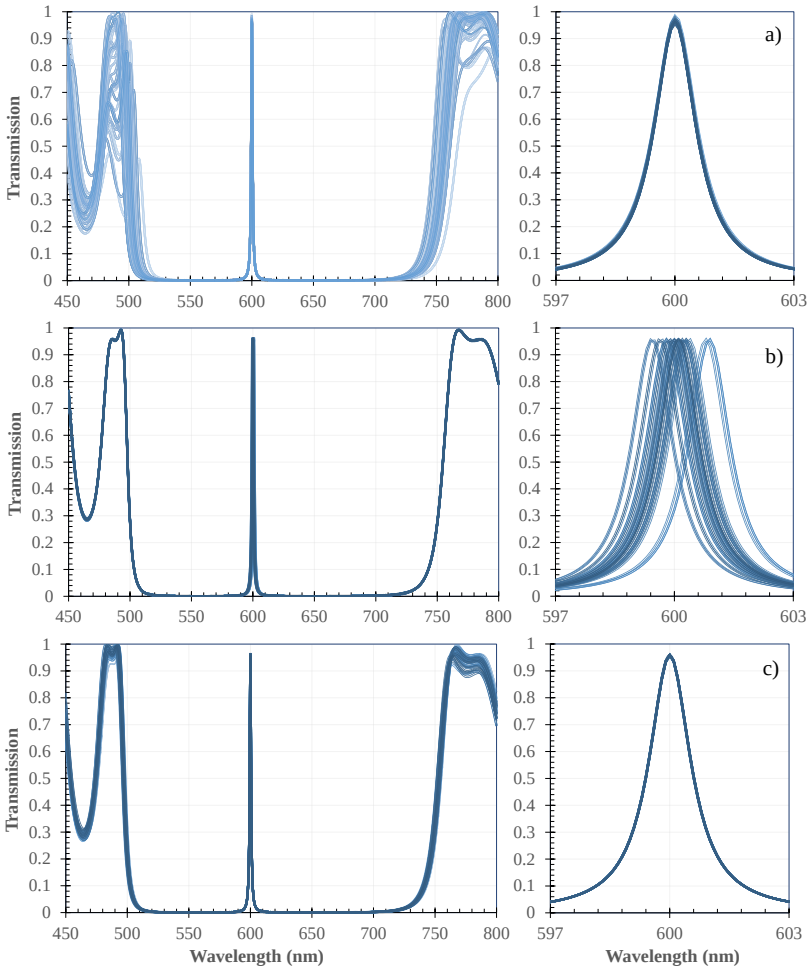


Fig. 4 Left: simulation of the final spectral performances in the 450-800 nm range of a filter monitored with a) TPM, b) POEM and c) Hybrid monitoring (30 predictions). Right: zoom within the bandpass region around 600 nm.

In order to have a global vision of the expected results of such single cavity filter for the three proposed strategies, we plotted in Fig. 4 the spectral dependence of transmission for 30 predictions using a) TPM, b) POEM and c) hybrid on the 450-800 nm range with a zoom near the bandpass domain around 600nm. This figure visually confirms the results given in Tables 2, 3 and 4. In particular, the spectral response outside bandpass and mirror rejection spectral domains (i.e. below 550 nm and above 700 nm) of a filter simulated with TPM strategy is quite unstable and very different from the nominal filter. This may be problematic if other optical functions (antireflective, low pass or high pass for example) need to be combined with the Fabry-Perot filter by deposition of additional layers monitored outside the 550 nm-700 nm spectral region.

### *2.3 Second example: two cavity Fabry-Perot filter*

This hybrid method can be generalized to multiple cavity filters. We are now considering the same filter duplicated with a low index L coupling layer between the two cavities. The corresponding formula of this 43-layer filter is

$$Glass\left|\ (HL)^5\ 2H\ (LH)^5\ L\ (HL)^5\ 2H\ (LH)^5\right|Air. \qquad (5)$$

It is well known that such a filter is more critical than the previous one. An un-adapted strategy could lead to a modification of the transmittance spectral shape and a decrease of the maximum of transmittance value as soon as both filters do not present strictly identical centering wavelengths. For such a filter, the classical approach consists in monitoring the filter with TPM except for the layers where the method sensitivity is limited (i.e. the coupling layer and also the spacer layers and the mirror layers close to it) where time or quartz monitoring is applied. Similarly to single cavity Fabry-Perot filter, it is thus possible, to obtain a good filter centering but a limited broadband spectral agreement. We thus developed a hybrid technique based on the results of section 2.2. This optimal strategy consists in monitoring the first cavity by a 497 nm POEM (layers 1 to 14) / 600 nm TPM (layers 15 to 21) exactly as for the single cavity Fabry-Perot filter. The coupling layer (layer 22) is monitored by a quartz monitoring with a standard deviation of 2 nm. The following two layers (layers 23 and 24) are then monitored with 600 nm TPM strategy to correct phase errors which have been introduced by quartz monitoring of the coupling layer. Then, statistical simulations similar to the one in Fig. 3, have shown that layers 25 to 38 can be POEM monitored at 446 nm without any noticeable degradation of the phase. Indeed, this wavelength enables to maintain $\varphi_{RMSD}$ below 4 degrees, which is lower than with TPM. Finally, layers 39 to 43 are monitored with a 600 nm TPM in order to ensure the filter centering.

To illustrate how this hybrid monitoring strategy allows securing both low errors on every single layer and on the phase, we have plotted in Fig. 5 the evolution of $\varphi_{RMSD}$ versus layer number. The value of $\varphi_{RMSD}$ is maintained below 7 degrees for every layer.

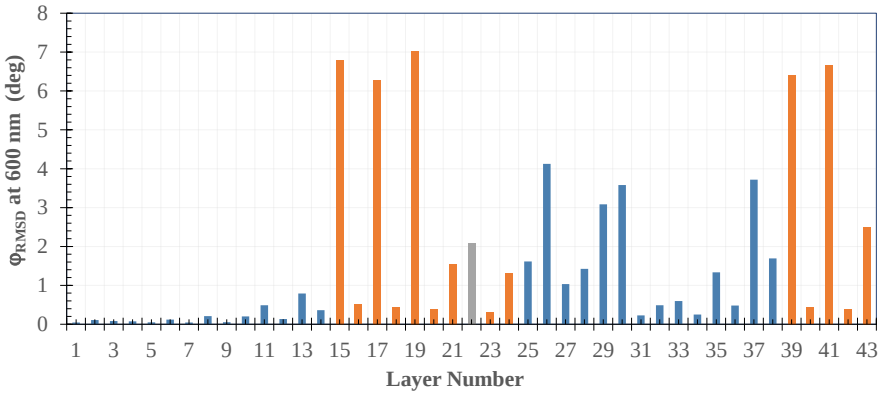


Fig. 5. Evolution of φRMSD at 600 nm following the described hybrid strategy applied to the two cavity filter. Grey rectangles correspond to Quartz monitoring, orange one to TPM and blue one to POEM.

Table 5 gives a comparison of the values of the 9 parameters for the nominal filter, a TPM strategy (with the coupling layer, the spacer layers and the mirrors layers surrounding the spacer layer monitored with a 2 nm standard deviation quartz), and our hybrid strategy. As for the single cavity filter, the hybrid strategy allows achieving similar performance as a TPM inside the transmittance window but also a better agreement with the nominal filter over a

broad spectral range (Fig. 6). The improvement of the spectral performances is not as good as the one achieved using hybrid strategy with single Fabry-Perot cavity. This is associated with the fact that the filter complexity is increased and therefore more sensitive to production errors. However, the gain of using hybrid strategy versus TPM is clearly visible and measurable.

**Table 5. Comparison of parameters value using TPM and Hybrid strategy. The statistical data are obtained using 100 predictions.**

| | | $\lambda_0$ nm | $T(\lambda_0)$ 0-1 | $FWHM_\lambda$ nm | $\lambda_{min1}$ nm | $T(\lambda_{min1})$ 0-1 | $\lambda_{min2}$ nm | $T(\lambda_{min2})$ 0-1 | $\lambda_a$ nm | $\lambda_b$ nm |
|---|---|---|---|---|---|---|---|---|---|---|
| | **Nominal Values** | **600** | **0.974** | **0.999** | **559.7** | **$9.0\ 10^{-8}$** | **646.8** | **$9.6\ 10^{-8}$** | **511.24** | **726.06** |
| **TPM** | Mean Value | 600.006 | 0.974 | 1.011 | 559.37 | $8.69\ 10^{-8}$ | 646.17 | $8.7\ 10^{-8}$ | 500.69 | 724.94 |
| | Difference | (0.006) | (<0.001) | (0.012) | (-0.326) | ($-3.1\ 10^{-9}$) | (-0.633) | ($9.\ 10^{-9}$) | (-10.55) | (-1.122) |
| | 2 × Standard deviation | 0.024 | 0.012 | 0.024 | 1.004 | $1.86\ 10^{-8}$ | 1.166 | $2.0\ 10^{-8}$ | 63.4 | 2.974 |
| **Hybrid** | Mean Value | 600.008 | 0.974 | 1.004 | 559.75 | $9.04\ 10^{-8}$ | 646.54 | $9.43\ 10^{-8}$ | 511.49 | 726.19 |
| | Difference | (0.008) | (<0.001) | (0.005) | (0.05) | ($4.\ 10^{-10}$) | (-0.264) | ($1.7\ 10^{-9}$) | (0.249) | (0.159) |
| | 2 × Standard deviation | 0.016 | 0.002 | 0.006 | 0.362 | $7.2\ 10^{-9}$ | 0.342 | $5.4\ 10^{-9}$ | 0.658 | 0.54 |

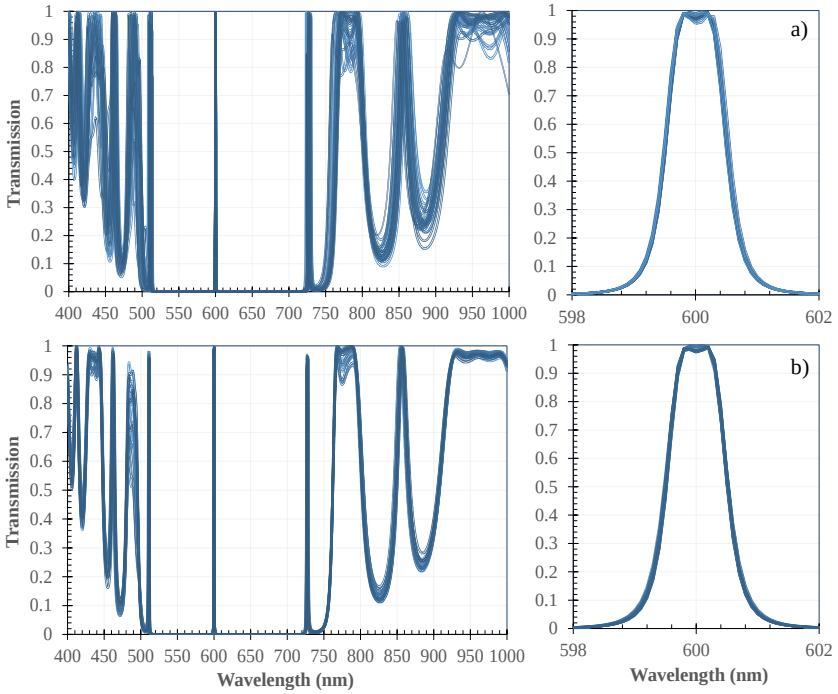


Fig. 6 Simulation of the final spectral performances in the 590-610 nm range of a filter fabricated with a) TPM and b) Hybrid monitoring (30 predictions).

## *2.4 Third example: a non-conventional three cavity filter*

We further investigated how our hybrid approach can be applied to other types of non-quaterwave bandpass structures. R. Willey proposed in [20] to design and monitor narrow bandpass filters with an asymmetrical ratio between high and low refractive index layer. One example of a 45-layer filter was given using a 4:1 ratio between the overall layer pair thickness and the thinnest individual layer. The design was the following:

$$\begin{aligned} &Glass \mid (0.5H\ 1.5L)^3\ 3.632H\ (1.5L\ 0.5H)^3\ 1.345L \\ &(0.5H\ 1.5L)^3\ 3.632H\ (1.5H\ 0.5H)^3\ 1.345L\ (0.5H\ 1.5L)^3 \\ &3.632H\ (1.5L\ 0.5H)^2\ 1.19989L\ 0.96265H\ 0.90522L \mid air. \end{aligned} \quad (6)$$

where glass refractive index is equal to 1.45, H index is fixed to 2.35 and L index is fixed to 1.45. According to R. Willey, the advantage of such an asymmetrical ratio filter is the ability to monitor it at the central wavelength, i.e. outside turning points where the sensitivity of the signal with thickness is very poor. The nominal strategy, derived from the one described in [18], consisted in monitoring all possible layers with POEM at the central wavelength, here supposed to be 600 nm (strategy POEM-1). However, POEM cannot be applied for some specific layers, e.g. layers 14 and 28: the signal sensitivity with thickness is too weak and layers 27, 40, 41 and 42: the vicinity of a turning point is not compatible with POEM. For these 6 layers, a quartz monitoring with a standard deviation of 2 nm was considered. As for previous filters, a statistical approach assuming a Gaussian noise with standard deviation $\sigma_{Transmittance} = 0.006$ on the transmitted signal was performed on 100 predictions. Some parameters including the centering wavelength, the maximum of transmittance and the $FWHM_\lambda$ were compared with the ideal filter. Table 6 lists the obtained values, and, in particular, one can see a noticeable standard deviation of the central wavelength of 0.23 nm. In fact, monitoring the filter at the central wavelength did not ensure the stability of the centering wavelength as POEM is not a phase compensation technique, even when it is used at the centering wavelength of the filter. Following the ideas developed for hybrid strategies in previous paragraphs, we decided to look for monitoring wavelengths able to minimize the phase root mean square deviation ($\varphi_{RMSD}$) at 600 nm, layer after layer (strategy POEM-2). One can show that for a POEM using 596 nm as a monitoring wavelength, the $\varphi_{RMSD}$ value at 600 nm remains below 1.7 degrees for layers 1 to 37 and then quickly diverges. To overcome this divergence, a second POEM wavelength must be determined for monitoring the last 5 layers. Minimal final $\varphi_{RMSD}$ value equal to 10.3 degrees is achieved if 605 nm is used as POEM wavelength for the last 5 layers of the filter. It can be noted that changing monitoring wavelength at this specific 38$^{th}$ layer is also interesting as, at a wavelength of 605 nm, this layer presents one maximum and one minimum transmittance value during the layer deposition, allowing POEM to more accurately recalibrate its signal levels.

**Table 6. Comparison of parameters value using POEM and Hybrid strategy.**

| | | $\lambda_0$, nm | $T(\lambda_0)$, 0-1 | $FWHM_\lambda$, nm |
|---|---|---|---|---|
| | **Nominal Values** | **600** | **0.998** | **12.28** |
| **POEM-1** | Mean Value | 599.98 | 0.998 | 12.28 |
| | Difference | (-0.018) | (<0.001) | (<0.001) |
| | 2 × Standard deviation | 0.46 | 0.0013 | 0.1 |
| **POEM-2** | Mean Value | 600.025 | 0.998 | 12.25 |
| | Difference | (0.025) | (<0.001) | (-0,029) |
| | 2 × Standard deviation | 0.048 | <0.001 | 0.044 |

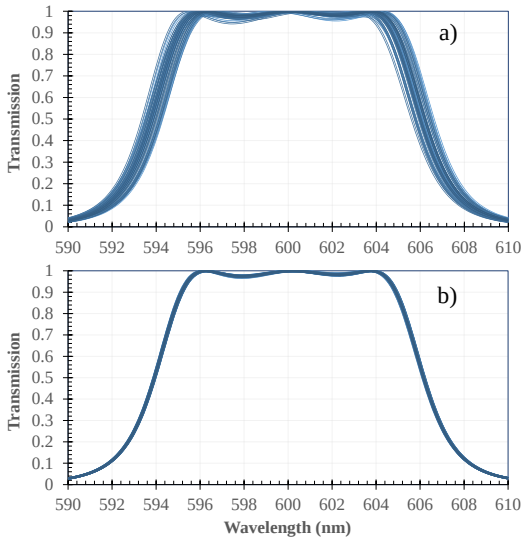


Fig. 7. Simulation of the final spectral performances in the 590-610 nm range of a filter fabricated with a) POEM and b) Hybrid monitoring (30 predictions).

Using the same approach and parameters as the one for classical Fabry-Perot filter, we calculated in Table 6 the performances of the filters obtained with both POEM-1 and the optimized POEM-2 strategies. One can see that POEM-2 strategy provides very stable filters' parameters and in particular a low standard deviation of the central wavelength of about 0.024 nm. We have plotted in Fig. 7 the spectral dependence of the transmission for 30 predictions using the two described strategies. Noticeable lower deviation between nominal and simulated transmission is observed when moving from POEM to hybrid strategy.

## 3. Conclusion

Even if optical thin film technology made great improvement over the last decades, the accurate manufacturing of narrow band pass filters still remains of first importance. Turning Point Monitoring remains till today the most common strategy for monitoring quaterwave based structures. However, the associated errors may lead to unwanted spectral discrepancies, like an incorrect rejection bandwidth or unwanted parasitic peaks for complicated designs mixing dichroic and bandpass filters. Another interesting technique is Percent Optical Extremum Monitoring. When the monitoring wavelength is judiciously selected, this method is particularly efficient for minimizing the average thickness error of each individual layer during deposition, and a quite good agreement between measured and calculated spectral transmittance can be expected over a broad spectral range. However, this technique shows limitations when perfect filter centering is required as for narrow bandpass filter. We have thus proposed a hybrid strategy combining strengths of both monitoring strategies. POEM was used as a low thickness error method, as soon as the filter centering is not critical or the cumulative errors of each individual layer thickness remain small enough. When such condition is no longer fulfilled, TPM is used as it enables correcting the filters centering. In the case of non-quarter wave designs, we proposed a similar approach, based on the phase value calculated at the centering wavelength layer after layer. In this case, only POEM is used to monitor the filters and the selected wavelengths ensures a good centering of the final filter.

## 4. Acknowledgments

This work was performed within the LabTOP (Laboratoire Commun de Traitement Optique des surfaces) a research cooperation agreement between AMU/CNRS/ECM/Institut Fresnel and CILAS Company.